Molecular Crystals and Liquid Crystals Science and Technology. Section A. Molecular Crystals and Liquid Crystals

Publication details, including instructions for authors and subscription information:
http://www.tandfonline.com/loi/gmcl19

Effect of Director Pretilt on Field Induced Periodic Distortions in Nematics

U. D. Kini [a]

[a] Raman Research Institute, Bangalore, 560 080, India

Version of record first published: 04 Oct 2006

To cite this article: U. D. Kini (1997): Effect of Director Pretilt on Field Induced Periodic Distortions in Nematics, Molecular Crystals and Liquid Crystals Science and Technology. Section A. Molecular Crystals and Liquid Crystals, 308:1, 43-76

To link to this article: http://dx.doi.org/10.1080/10587259708045094

Mol. Cryst. Liq. Cryst., 1997, Vol. 308, pp. 43–76
Reprints available directly from the publisher
Photocopying permitted by license only

Effect of Director Pretilt on Field Induced Periodic Distortions in Nematics

U. D. KINI

Raman Research Institute, Bangalore - 560 080, India

(Received 26 February 1997)

This work reports a theoretical study on the linear threshold of static director distortions in a rigidly anchored nematic sample subjected to the simultaneous actions of electric (**E**) and magnetic (**B**) fields applied along certain symmetry directions with respect to the initial uniform director alignment $\mathbf{n}_0$. The results mainly concern a material having susceptibility anisotropies of opposite signs ($\varepsilon_A > 0$, $\chi_A < 0$). The deformation above the electric threshold may be homogeneous (HD) or periodic (PD) depending upon material and geometric parameters. *PD* is quenched when $\mathbf{n}_0$ is tilted sufficiently away from the homeotropic or when **B** is impressed away from **E**. For a given director pretilt, the direction of post threshold periodicity changes continuously with the magnetic tilt. At a given magnetic tilt, the *PD* threshold parameters exhibit a discontinuous change when the director pretilt is varied. Phase diagrams in different planes of the parameter space demarcate the regions of existence of *PD* and *HD*. The importance of elastic anisotropy in determining the nature of *PD* emerges from a study of a hypothetical material having two equal curvature elastic constants.

Keywords: Electric and magnetic field effects on liquid crystals; orientational transitions in liquid cyrstals; curvature elasticity of liquid crystals; boundary value and eigenvalue problems; numerical simulation, solution of differential equations; stability and perturbation methods

1. INTRODUCTION

The application of destabilizing orienting fields along suitable directions with respect to an aligned nematic sample leads to the symmetry breaking Freedericksz transition above which the director field suffers deformations of different kinds. These distortions are well explained by the continuum theory [1–4]. The nature of the distortion may be periodic (*PD*) or homogeneous (*HD*) depending upon factors such as material parameters, field directions, director pretilt at the substrates, etc. The aperiodic *HD* is uniform in the sample plane and appears in materials having moderate elastic

anisotropy. In nematics with high elastic anisotropy, *PD* appears above a well defined magnetic threshold [5]. Effects of **E** are more complicated than those of **B** due to modifications of the field inside the sample [6]. The presence of flexoelectricity [7] causes *PD* to appear even in nematics with low elastic anisotropy [8]. A high frequency **E** field may lead to *PD* in some materials exhibiting dielectric relaxation [9]. A deformation that sets in initially may change into a distortion of an other kind when the destabilizing field strength is raised above the first transition. Close to the nematic-smectic A transition, increase of B in the bend geometry causes the appearance of first *HD* and then *PD* [10]. *PD* that sets in above a magnetic threshold in some polymer nematics can be quenched discontinuously into *HD* by raising B above the *PD* threshold [11]. A subsequent decrease in the magnetic field causes a hysteretic restoration of *PD*.

Hysteresis and discontinuous changes in deformation also occur in crossed field configurations in which **E** and **B** are applied with **E** in the sample plane. In *5CB* (nematic with positive dielectric and diamagnetic anisotropies; $\varepsilon_A > 0$ an $\chi_A > 0$, respectively), *HD* appears discontinuously above the bend electric threshold when the stabilizing **B** field is not strong [12]. When **B** is strong enough, the distortion that appears above the transition is periodic and is preceded by pretransitional optical biaxiality [13]. A simple non-linear perturbation model qualitatively accounts for the appearance of *PD* with periodicity along **E** [14]. A linear perturbation model [15] also explains some of the observed features of *PD* studied in ref.s 12 and 13. It is also shown [15] that *PD* may occur with periodicity in a direction normal to **E**. The linear model has been extended [16] to the study of *PD* in homeotropically aligned samples of materials (such as *M1* [17] and *CCH* -7 [18]) having opposite signs of susceptibility anisotropies. It is shown [16] that the direction of periodicity in the sample plane may change continuously (for *CCH* -7) or discontinuously (for *M1*) when the direction of **B** is varied in the sample plane. The linear model has been extended [19] to the case of $\mathbf{n}_o$ pretilted away from the homeotropic in a plane normal to **E**. It is found [19] that *PD* in *M1* or *5CB* is quenched in favour of *HD* when $\mathbf{n}_o$ is tilted sufficiently away from the homeotropic. Calculations also show [19] that *PD* may be suppressed by rotating **B** away from **E** in a plane normal to $\mathbf{n}_o$.

Due to the rather different solutions obtained for *CCH* -7 parameters in the homeotropic case [16], it appears interesting to investigate how the *PD* threshold in this material gets influenced by director pretilt. Motivated thus, the linearized governing equations describing *PD* and *HD* are set up along with the relevant boundary conditions in section 2; the *HD* threshold is also

briefly discussed. Sections 3 and 4 contain results on the *PD* threshold and its comparison with the *HD* threshold for real nematic parameters. Section 5 concludes the discussion and indicates the limitations of the present calculations from the theoretical as well as the experimental viewpoints. Recent studies on a discotic nematic [20] as well as on nematic mixtures [21] indicate the possibility of preparing materials having exotic elastic and dielectric properties. Keeping this in mind, sections 3.2 and 4.2 carry brief discussions on materials with different types of elastic anisotropy.

2. GOVERNING EQUATIONS, BOUNDARY CONDITIONS, *HD* THRESHOLD

A brief derivation is presented (for details, see section 2 of ref. 19). A nematic insulator of thickness $2h$ is confined between isotropic dielectric plates $z = \pm h$ and sandwiched between flat electrodes $x = \pm g$ lying in the yz plane. The electrode gap $2g$ is large compared to the sample thickness $2h$ and the sample is studied near $x = 0$, away from both electrodes. A potential difference V_o is applied betwen the electrodes. The initial uniform director orientation in the yz plane makes an angle ϕ_o with the z axis:

$$\mathbf{n}_o = (0, S, C); S = \sin \phi_o,\ C = \cos \phi_o;\ \phi_o = \text{constant}.$$

The range $0 \leqslant \phi_o \leqslant \pi/2$ can be fixed for the pretilt angle without loss of generality. The magnetic intensity is in a plane normal to $\mathbf{n}_o$ with

$$\mathbf{H}_\perp = (H_\perp C_\alpha, H_\perp S_\alpha,\ -H_\perp S_\alpha S)$$

where $S_\alpha = \sin \alpha$ and $C_\alpha = \cos \alpha$. Inside the sample, the unperturbed, uniform $\mathbf{E}$ field is $\mathbf{E}_o = (E_{xo}, 0, 0)$ with $E_{xo} = V_o/2g$. Clearly, x axis is a symmetry direction for the sample. The perturbed director and $\mathbf{E}$ fields are

$$\mathbf{n} = [\sin \theta,\ \cos \theta \sin (\phi_o + \phi),\ \cos \theta \cos (\phi_o + \phi)];$$

$$\mathbf{E} = \mathbf{E}_o + \mathbf{E}';\quad \mathbf{E}' = -\nabla \psi \tag{1}$$

where the perturbations θ, ϕ, ψ are functions of x, y, z; Maxwell's curl equation enables writing $\mathbf{E}'$ as the gradient of the scalar potential ψ. For

linear perturbations, the total free energy density (at fixed voltage between electrodes) is

$$F=\frac{1}{2}\Big[K_1(\theta_{,x}+C\phi_{,y}+S\phi_{,z})^2+K_2(\phi_{,x}-C\theta_{,y}+S\theta_{,z})^2$$

$$+K_3\{(S\theta_{,y}+C\theta_{,z})^2+(S\phi_{,y}+C\phi_{,z})^2\}$$

$$-\frac{1}{4\pi}\{\varepsilon_\perp(\psi_{,x}^2+\psi_{,y}^2+\psi_{,z}^2)+\varepsilon_A(E_{xo}\theta-S\psi_{,y}-C\psi_{,z})^2\}\Big]$$

$$-\frac{\chi_A H_\perp{}^2}{2}(C_z\theta+S_z\phi)^2 \tag{2}$$

where K_1, K_2 and K_3 are the splay, twist and bend elastic constants, respectively; $\varepsilon_\parallel$, $\varepsilon_\perp$ are, respectively, the dielectric constants parallel to and normal to the director so that $\varepsilon_A=\varepsilon_\parallel-\varepsilon_\perp$; a subscripted comma denotes partial differentiation. The neglect of flexoelectricity may be a reasonable assumption if $\mathbf{E}_o$ is an *ac* field with sufficiently high frequency; then, E_{xo} is identified with the *rms* value. Maxwell's divergence equation results by minimizing the total free energy with respect to ψ holding other quantities constant:

$$\operatorname{div}(\mathbf{D})=-[\varepsilon_\perp\psi_{,xx}+(\varepsilon_\perp+\varepsilon_A S^2)\psi_{,yy}+2\varepsilon_A SC\psi_{,yz}+f_3\psi_{,zz}]$$

$$+\varepsilon_A E_{xo}(S\theta_{,y}+C\theta_{,z})=0;\ f_3=\varepsilon_\perp+\varepsilon_A\ C^2 \tag{3}$$

where $\mathbf{D}$ is the electric displacement. Variations of the total free energy with respect to θ and ϕ lead to the torque equations:

$$K_1\theta_{,xx}+(K_2C^2+K_3S^2)\theta_{,yy}+f_1\theta_{,zz}+2\ (K_3-K_2)SC\theta_{,yz}$$

$$+\theta\left(\frac{\varepsilon_A E_{xo}^2}{4\pi}+\chi_A H_\perp^2 C_z^2\right)+\chi_A H_\perp^2 S_z C_z\phi+(K_1-K_2)(\phi_{,xy}C-\phi_{,xz}S)$$

$$-\frac{\varepsilon_A E_{xo}}{4\pi}(\psi_{,y}S+\psi_{,z}C)=0;\ f_1=K_2S^2+K_3C^2 \tag{4}$$

$$K_2\phi_{,xx} + (K_1C^2 + K_3S^2)\phi_{,yy} + f_2\phi_{,zz} + 2(K_3 - K_1)SC\phi_{,yz}$$

$$+ \chi_A H_\perp^2 S_\alpha^2 \phi + \chi_A H_\perp^2 S_\alpha C_\alpha \theta + (K_1 - K_2)(\theta_{,xy}C - \theta_{,xz}S) = 0;$$

$$f_2 = (K_3C^2 + K_1S^2). \tag{5}$$

The boundary conditions are now formulated. The importance of interfacial effects in determining director distortions is well known [22]. Possible effects of finiteness of director anchoring strengths on *PD* have also been studied [23]. When the director field in the sample bulk is deformed, the elastic torques tend to change the director orientation away from the direction of anchoring as the surface anchoring energy is finite. Realistic boundary conditions for θ and ϕ result only from the balance equation of the surface torque. This is not attempted here as both the polar and the azimuthal anchoring strengths enter the picture as additional parameters. For the sake of simplicity, the rigid anchoring hypothesis is adopted so that the director perturbations are assumed to vanish at the sample planes. According to the electromagnetic theory [24], D_z, the normal component of **D** is continuous at the sample plates. This implies that D_z must also vanish at the boundaries. Hence, the boundary conditions take the form

$$\theta(z = \pm h) = 0; \quad \phi(z = \pm h) = 0;$$

$$\varepsilon_A C E_{xo}\theta - \varepsilon_A SC\psi_{,y} - f_3\psi_{,z} = 0 \text{ at } z = \pm h. \tag{6}$$

As the magnetic torque is proportional to $H_\perp^2$, $H_\perp$ can be taken positive. Equations (3)–(6) are invariant under the transformation $E_{xo} \to -E_{xo}$, $\psi \to -\psi$. Hence, E_{xo} can be assumed to be positive. Similarly, the transformation $\alpha \to \pi + \alpha$ leaves (3)–(6) unchanged; hence, the range $0 \leqslant \alpha \leqslant \pi$ seems sufficient for discussing the results. It is shown presently (section 4) that half of this range is adequate so that the y axis can also be treated as a symmetry direction in the sample.

As is clear, any solution of the governing equations (3)–(6) leads to an eigenvalue problem in which the absolute magnitudes of the perturbations are not known. Depending upon the assumptions relating to the spatial variation of the perturbations, a subset of terms from (3)–(6) is chosen for solution. In some cases, the boundary conditions (6) may even cause one of the perturbations to vanish. As the governing equations are linear and the sample limited only along z, the variation along x or y can be assumed to be periodic. **Four** different kinds of instabilities can be studied. These are [25]:

HD. Homogeneous or aperiodic distortion. Perturbations depend only on z.
X Mode. Perturbations vary only with x and z. Periodicity is along x.
Y Mode. Perturbations depend on y and z. Periodicity is along y.
XY Mode. Perturbations vary with x, y and z. Periodicity is in the xy plane at some angle with the x axis.

We are interested in the calamitic material $CCH-7$ with typical parameters [18]

$$(K_1, K_2, K_3) = (7.25, 3.48, 11.46)\,10^{-7}\,\text{dyne};$$

$$\chi_A = -3.22\,10^{-8}\,\text{emu};\ \varepsilon = 8.01;\ \varepsilon_\perp = 3.72;\ \varepsilon_A = 4.29. \tag{7}$$

As ε_A is positive, $\mathbf{E_0}$ acts as a destabilizing field; hence, we look for the electric threshold. As χ_A is negative, $\mathbf{H}_\perp$ can lend a stabilizing influence if it is impressed in a plane normal to $\mathbf{n}_0$.

In general, all three perturbations are associated with HD. The boundary conditions for HD become

$$\theta(z = \pm h) = 0;\ \phi(z = \pm h) = 0;\ \psi_{,z} = 0 \text{ at } z = \pm h. \tag{8}$$

Noting the modal structure of the equations, we seek solutions of the form

$$(\theta, \phi, \psi) = (\theta_A \cos qz, \phi_A \cos qz, \psi_A \sin qz) \tag{9}$$

where θ_A, ϕ_A and ψ_A are constant amplitudes; θ and ϕ are symmetric about the sample centre while ψ is antisymmetric. For HD, (3) integrates exactly along with (6) to enable expressing $\psi_{,z}$ in terms of θ. The compatibility of (4)–(5) and (8) leads to the electric HD threshold, E_F, with

$$E_F{}^2 = \frac{q^2(\sigma_E f_1 - \chi_A h^2 H_\perp^2 C_x^2)}{f_1 \sigma_E \sigma_D};\ q = \frac{\pi}{2};\ \sigma_D = \frac{\varepsilon_\perp \varepsilon_A h^2}{4\pi f_1 f_3};$$

$$\sigma_E = q^2 - \frac{\chi_A h^2 H_\perp^2 S_x^2}{f_2}. \tag{10}$$

The definition of σ_D indicates how the electric field perturbation associated with θ changes the effective dielectric anisotropy from ε_A to $\varepsilon_\perp \varepsilon_A / f_3$. Clearly, E_F of (10) is a function of both α and ϕ_0. The threshold for the uncoupled mode with opposite parity results from (9) if the value of q is doubled. It appears that this threshold is generally higher than that given by (10). When $\alpha = 0$, ϕ damps out as it lacks a driving torque to destabilize it. In this case, HD is associated with only θ and ψ and the HD threshold (10) increases

with $H_\perp$. At $\alpha = \pi/2$, ϕ again damps out because of χ_A being negative. But in this case, $\mathbf{H}_\perp$ does not affect the *HD* threshold for any pretilt ϕ_0.

3. RESULTS FOR A HOMEOTROPIC SAMPLE; $\phi_0 = 0$

Clearly, $S = 0$ and $C = 1$. Some of the earlier results (section 4 of ref. 16) are briefly recalled for completeness. Now, E_F of (10) becomes a function of α as $\mathbf{H}_\perp$ remains in the xy plane. The boundary conditions reduce to (8) for all four types of solutions. The mixed derivative terms disappear from the governing equations (3)–(5). Hence, the governing equations now support two uncoupled solutions for any of the four instabilities:

SOLUTION 1: θ and ϕ are even and ψ is odd.
SOLUTION 2: θ and ϕ are odd and ψ is even.

SOLUTION 1 is an extension of *HD* with the threshold (10); hence, SOLUTION 1 is studied. For the *XY* Mode, the *ansatz*

$$(\theta, \phi, \psi) = \left(\theta_A \cos\frac{qz}{h},\ \phi_A \cos\frac{qz}{h},\ \psi_A \sin\frac{qz}{h}\right) \sin\left(\frac{Q(x\,C_\mu + y\,S_\mu)}{h}\right) \tag{11}$$

is substituted into (3)–(5); Q is a dimensionless wavevector magnitude and μ the angle between the wavevector and the x axis. The compatibility of (3)–(5) and (8) yields the requistie relation $E_{xo}(Q, \mu)$ expressing, E_{xo} as a function of Q and μ and other parameters such as $H_\perp$, h, the elastic constants and the susceptibilities:

$$\left(\frac{\varepsilon_A\,\varepsilon_\perp\,h^2}{4\pi K_3\,\varepsilon_\parallel}\right) E_{xo}^2(Q,\mu) = \frac{t_1 Q^6 + t_2 Q^4 + t_3 Q^2 + t_4}{u_1 Q^4 + u_2 Q^2 + u_3};$$

$$\beta_1 = \frac{K_1}{K_3};\ \beta_2 = \frac{K_2}{K_3};\ \beta_3 = \frac{\varepsilon_\perp}{\varepsilon_\parallel};\ \sigma_H = \frac{\chi_A h^2 H_\perp^2}{K_3};$$

$$u_1 = j(\mu) = \beta_2 C_\mu^2 + \beta_1 S_\mu^2; t_1 = \beta_3\beta_2\beta_1;\ q = \frac{\pi}{2};$$

$$t_2 = q^2[\beta_1\beta_2 + \beta_3(\beta_1 + \beta_2)] - \sigma_H\beta_3 j(\alpha - \mu);$$

$$t_3 = q^2[q^2(\beta_3 + \beta_1 + \beta_2) - \sigma_H\{\beta_3 + j(\alpha - \mu)\}];\ t_4 = q^4(q^2 - \sigma_H);$$

$$u_2 = q^2[j(\mu) + 1] - \sigma_H S_\alpha^2;\ u_3 = q^2(q^2 - \sigma_H S_\alpha^2). \tag{12}$$

Clearly, $E_{xo}(0,\mu)$ equals the *HD* threshold, E_F. For a given material, $H_\perp$ and sample thickness, $E_{xo}(Q,\mu)$ defines a neutral stability surface. If $E_{xo}(Q,\mu)$ exhibits a minimum $E_P = E_{xo}(Q_P,\mu_P)$, then Q_P is the **dimensionless wavevector** at XY mode threshold and μ_P the **angle between the wavevector and** x **axis at the** XY **threshold**. The X and Y Modes can be regarded as particular cases of the XY Mode. The Y Mode is studied by putting $\mu = \pi/2$ in (11) and (12). Then, the Y threshold is the minimum $E_{PY} = E_{xo}(Q_{PY},\pi/2)$ of the neutral stability curve $E_{xo}(Q,\pi/2)$ that results from a projection of the neutral stability surface on the plane $\mu = \pi/2$. In the same way, the X threshold results as the minimum $E_{PX} = E_{xo}(Q_{PX},0)$ of the neutral stability curve $E_{xo}(Q,0)$. By doubling the value of q in (12), the threshold for SOLUTION 2 can be determined; this threshold is generally higher than that of SOLUTION 1 (ie., SOLUTION 2 is less favourable than SOLUTION 1).

The dimensionless thresholds

$$R_P = \frac{E_P}{E_F}, R_X = \frac{E_{PX}}{E_F}, R_Y = \frac{E_{PY}}{E_F}$$

make possible a convenient way to measure the *PD* thresholds relative to the *HD* threshold. If, for instance, $R_P < 1$, the XY Mode is more favourable than *HD*. If the condition $R_P = 1$ is satisfied for a set of parameters, it defines the phase boundary between the XY Mode and *HD*. A similar statement can be made for the existence of the X and Y Modes relative to *HD*. The XY Mode may also have interfaces with the X and Y Modes. For instance, when $\mu_P \to 0$ (or when $\mu_P \to \pi/2$), the XY threshold equals the X (or the Y) threshold.

3.1. Results for Real Parameters

For parameters (7), typical results are summarized (see Fig. 4 of ref. 16; also, Fig. 1, Figs. 5a–5c). The XY Mode degenerates into the Y Mode when $H_\perp = 0$ and when $\mathbf{H}_\perp$ is impressed along the x axis ($\alpha = 0$) or along the y axis ($\alpha = \pi/2$). In all these cases, $R_Y < 1$ so that *HD* cannot appear. If $\mathbf{H}_\perp$ is strong enough, the X Mode is also more favourable than *HD* ($R_X < 1$) but $R_Y < R_X$ for any $H_\perp$; hence, the X Mode is of no real interest. Still, a study of the X Mode is useful in providing a measure for $H_\perp$. With $\mu = 0$ in (12), we expand $E_{xo}^2(Q,0)$ in powers of Q. To lowest order, $E_{xo}^2(Q,0) \approx E_F^2 + Q^2\delta$ where δ is proportional to $t_3u_3 - t_4u_2$. If $\delta < 0$, the X Mode is more favourable than *HD*. Clearly, $\delta = 0$ defines the critical point between the X Mode and *HD*. When $\mathbf{H}_\perp$ acts along x ($\alpha = 0$), the critical condition takes a simple

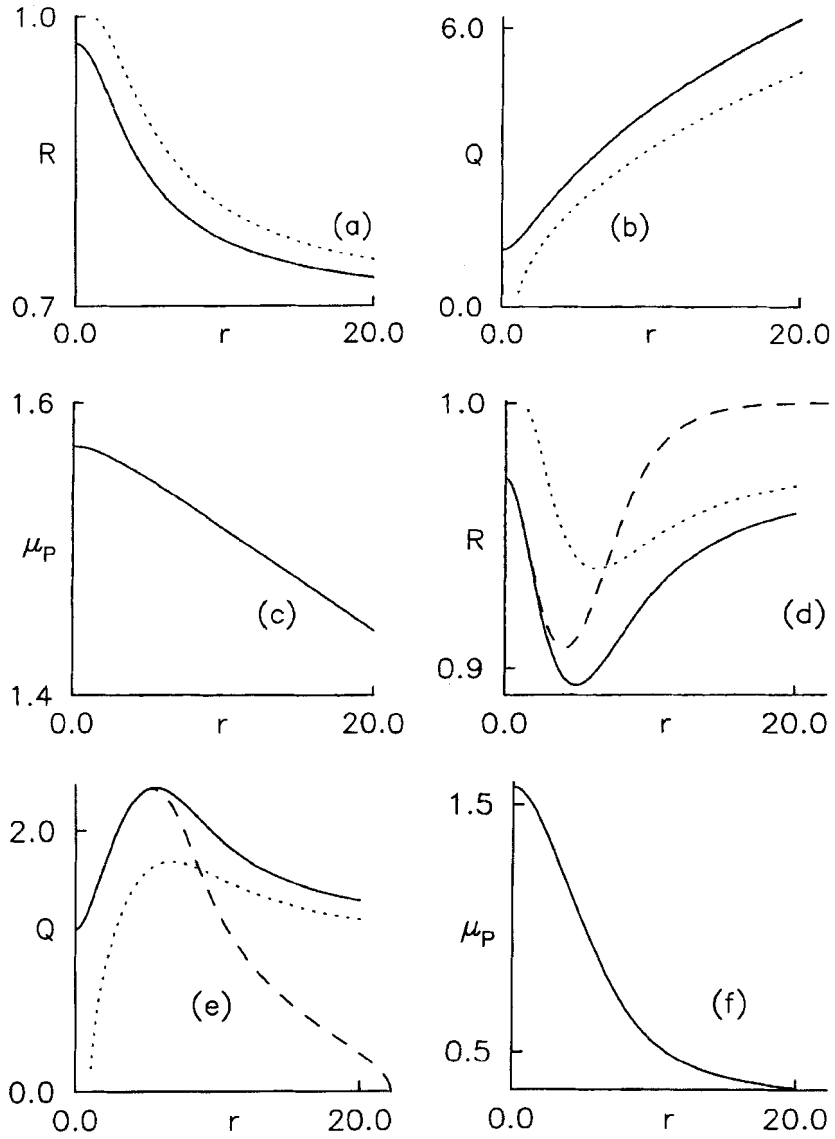

FIGURE 1 Plots of reduced electric *PD* thresholds (R_P, R_X, R_Y), dimensionless wavevector magnitudes (Q_P, Q_{PX}, Q_{PY}) and μ_P as functions of the dimensionless stabilizing magnetic strength r; μ_P is the angle between the XY Mode wavevector and the x axis (see Section 3 for definitions). XY Mode (—), Y Mode (----) and X Mode (....). Parameters used are (7). Director pretilt angle $\phi_o = 0.01$ radian ($\mathbf{n}_o$ is close to the homeotropic). The magnetic tilt angle $\alpha =$ (a, b, c) 0.01 (d, e, f) 0.3 radian. The XY Mode is the only favourable deformation. Increase of magnetic tilt causes an appreciable decrease in the wavevector (the stripes should become broader) at corresponding values of r. When $\mathbf{H}_\perp$ is close to the x axis (a, b, c), the XY Mode overlaps the Y Mode. At higher magnetic tilt (d, e, f), the XY Mode threshold and wavevector approach the corresponding Y Mode and X Mode parameter at low r and high r, respectively. In particular, $\mu_P \to \alpha$. when $\mathbf{H}_\perp$ is strong (Section 4). The results for the XY Mode are similar to those of Figures 4a–4c, ref. 16 (Section 3).

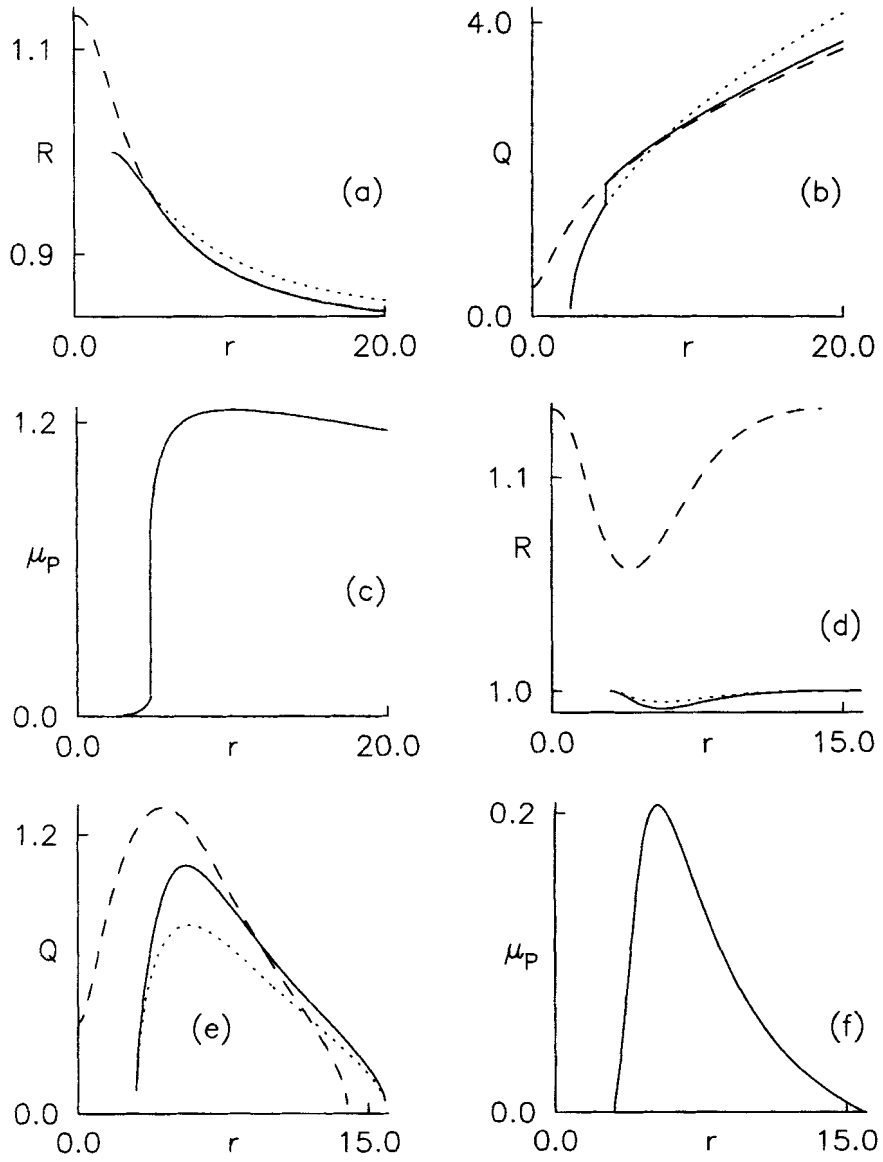

FIGURE 2 Details as in Figure 1 except that the director pretilt away from the homeotropic is high ($\phi_o = 0.8$) radian. The magnetic tilt angle α = (a, b, c) 0.01 (d, e, f) 0.3 radian. At low α (a, b, c), the XY Mode approaches the X Mode and gets quenched when $\mathbf{H}_\perp$ is weak enough; hence, HD should occur in the low r range. The change over of the XY Mode from the Y to the X Mode with decreasing r occurs via a discontinuity in R_P, Q_P and μ_P. Though the Y Mode exists as a solution in the low r range, it is of no real interest as $R_Y > 1$. At higher magnetic tilt (d, e, f), the Y Mode is of only academic interest as R_Y exceeds unity at all r. The XY Mode disappears at two cutoff values of r (Section 4).

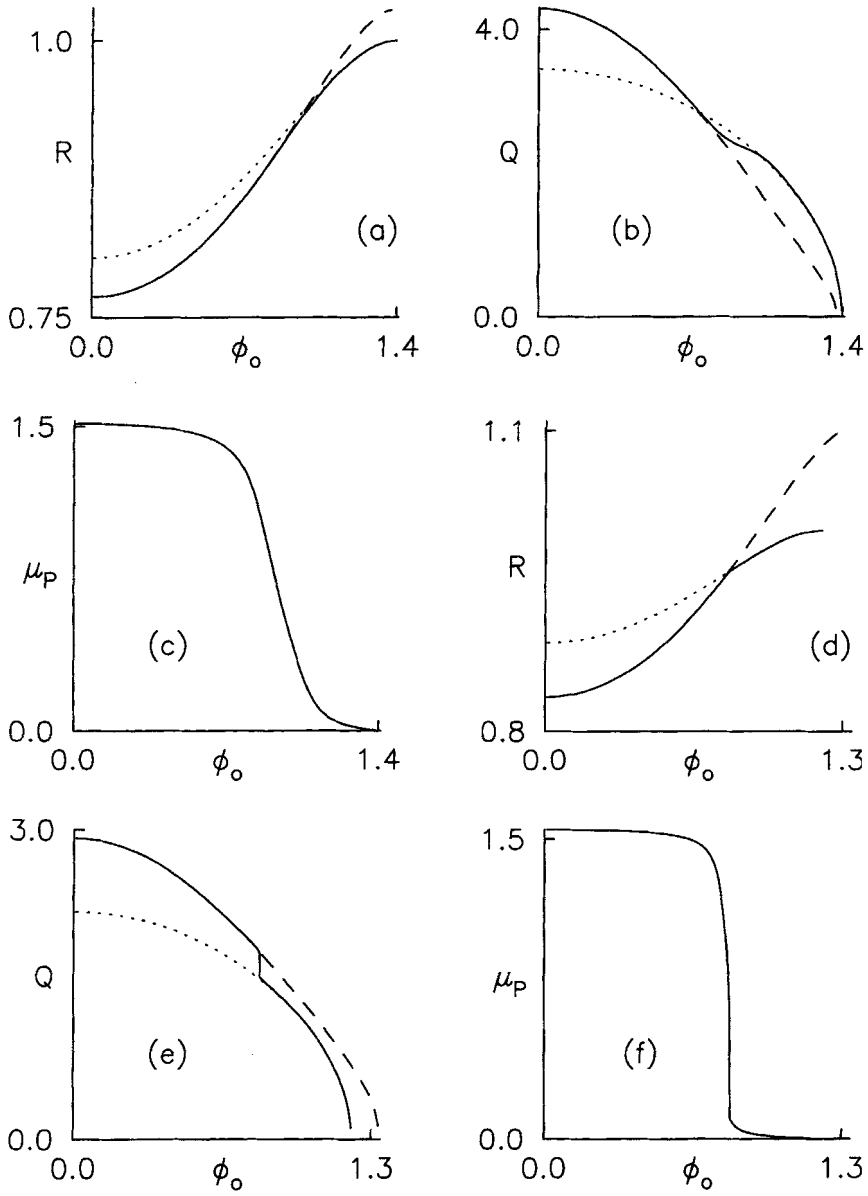

FIGURE 3 Plots of threshold parameters for the XY, X and Y Modes as functions of the director pretilt, ϕ_o when the stabilizing $\mathbf{H}_\perp$ is fixed (see Fig. 1 for details). The magnetic tilt $\alpha = 0.01$ radian; $\mathbf{H}_\perp$ is close to the x axis. The dimensionless magnetic strength $r =$ (a, b, c) 10 (d, e, f) 5. Increase of the director pretilt causes the XY Mode to damp out; HD should set in at sufficiently high ϕ_o. The behaviour of the XY Mode is similar to that of the Y Mode at low ϕ_o and that of the X Mode at high ϕ_o; the change over occurs continuously at high r (a, b, c) but discontinuously at low r (d, e, f). R_Y exceeds unity when the director pretilt is high (see Section 4).

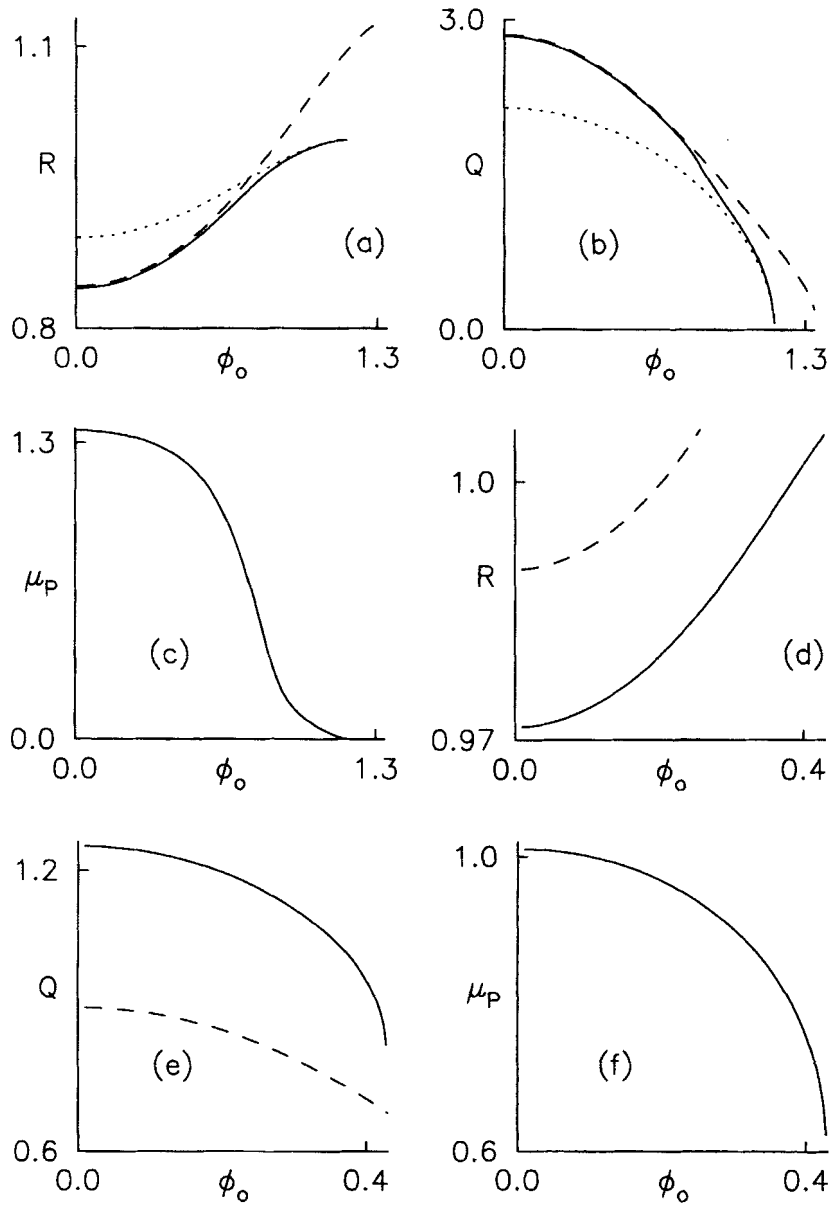

FIGURE 4 Details as in Figure 3 but with higher magnetic tilt away from the x axis. In (a, b, c), $r = 5$ and $\alpha = 0.1$ radian. The discontinuity seen in Figures 3d–3f is removed by increase in magnetic tilt. In (d, e, f), $r = 20$ and $\alpha = 1.0$. The X Mode does not exist at all even as a solution; the Y Mode exists but is completely seggregated from the XY Mode. The XY Mode quenching is discontinuous with respect to the wavevector (when $R_P = 1$, Q_P is non-zero) and μ_P also does not assume either of its symmetry values.

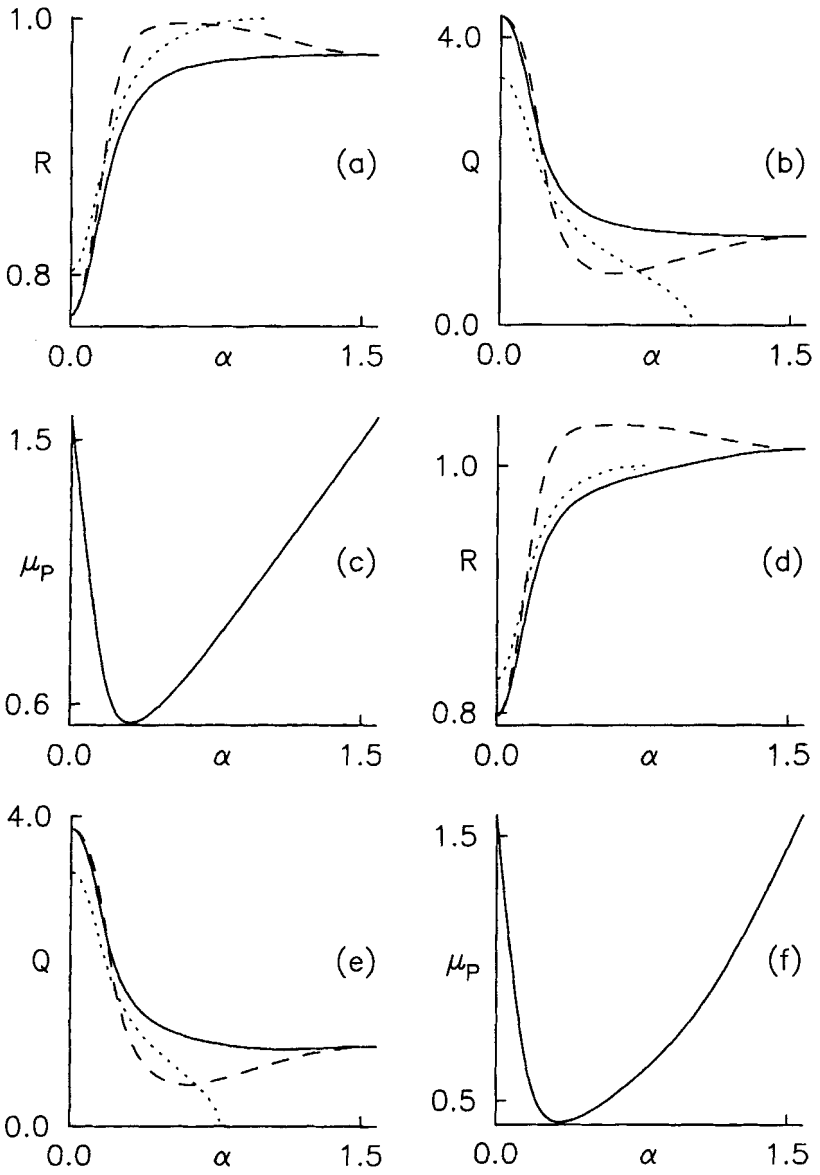

FIGURE 5 Variation of threshold parameters with the magnetic tilt α when the director pretilt ϕ_o and the reduced stabilizing magnetic strength r are held costant. $r = 10$. $\phi_o =$ (a, b, c) 0.01 (d, e, f) 0.4 radian. Results for the range $\pi/2 \leqslant \alpha \leqslant \pi$ are obtained by reflecting the diagrams (a, b, d, e) in the vertical mirror at $\alpha = \pi/2$; in the case of (c) and (f), this is followed by a further reflection in the horizontal line $\mu_P = \pi/2$. For low director pretilt (a, b, c), the XY Mode is favourable over the entire α range; at a higher pretilt (d, e, f), the XY Mode gets quenched discontinuously in favour of HD when $\mathbf{H}_\perp$ is rotated sufficiently away from the x axis; the periodicity direction of the XY Mode is nearer y than x (Section 4). Though the Y Mode exists as a solution in (d, e, f), R_Y exceeds unity over a major portion of the α range. Results of (a)–(c) are similar to those for the homeotropic orientation (Section 3).

form (see eqn. 27, ref. 16),

$$H_C^2 = -\frac{\varepsilon K_3 \pi^2}{4\varepsilon_A h^2 \chi_A}\left(\frac{K_1}{K_3} - \frac{\varepsilon_A}{\varepsilon}\right); \tag{13}$$

when $H_\perp$ is diminished to H_C, $Q_{PX} \to 0$. Now, $H_\perp$ can be measured in terms of H_C to yield the dimensionless magnetic intensity

$$r = \frac{H_\perp}{H_C}.$$

The results become independent of h if they are expressed in terms of the dimensionless fields r and R. When $\mathbf{H}_\perp$ is rotated away from the symmetry directions, the XY Mode is found to be uniformly more favourable than the Y and X Modes. At XY threshold, μ_P the angle between the wavevector and the x axis depends on both $H_\perp$ and α. A qualitative explanation of some of the above results is given as this will facilitate the understanding of the results of section 4.

Consider first the X Mode and HD. Let $\mathbf{H}_\perp$ act along x. HD is associated with the bend deformation and the stabilizing electric component E_z' (as $\varepsilon_A > 0$). The X Mode is accompanied by the bend and splay deformations as well as the electric perturbations E_z' and E_x'; ϕ gets decoupled and damps out. The stabilizing action of E_z' (which varies in phase with θ along x) as well as the appearance of the splay distortion should cause the free energy of the X Mode to exceed that of HD. But the destabilizing electric component $E_x' \sim Q\psi/h$ becomes stronger when the wavevector magnitude (Q) is large enough; this is not true of E_z'. Eqn. (3) shows that the amplitude of both electric perturbations $\sim E_{xo}$. This factor can be enhanced by the application of a stabilizing $\mathbf{H}_\perp$ (then, E_{xo} has to be higher at threshold). When $H_\perp$ is sufficiently high, the destabilizing influence of E_x' become strong at high Q; then, the X threshold becomes lower than the HD threshold. With increase of r, Q_{PX} increases and R_X diminishes. In the limit of high r, $Q_{PX} \sim \sqrt{r}$ and $R_X \to \sqrt{\beta_3}$. A similar argument suffices to account for the Y threshold being lower than the HD threshold. As the Y Mode is associated with bend and twist, the Y threshold is always lower than the X threshold at $\alpha = 0$. In the limit of high r, $R_Y \to \sqrt{\beta_3}$; hence, the Y and X Mode thresholds are close to each other when $\mathbf{H}_\perp$ is strong.

The form and existence of the critical field H_C (13) for the X Mode at $\alpha = 0$ has the following interpretation.

(i) The additional elastic stabilizing torque associated with the splay distortion has to be anulled by the destabilizing torques arising from the electric perturbations.
(ii) The dielectric term $(-\varepsilon_A/\varepsilon_\parallel)$ is opposed to the elastic term (K_1/K_3); this is a sign of the destabilizing action of the electric perturbation.
(iii) The relative dielectric anisotropy is not high enough; ie., $\varepsilon_A/\varepsilon_\parallel < K_1/K_3$.

If the opposite condition were to hold, H_C of (13) would cease to be real and the X threshold would turn out to be **lower** than the HD threshold even in the absence of $\mathbf{H}_\perp$.

This is precisely what happens for the Y Mode whose critical field has the same form as (13) except that K_2 replaces K_1. As $K_2 < K_1$ (7), the Y Mode and HD do not have a real critical field separating them; in other words, the Y threshold is lower than the HD threshold even when $\mathbf{H}_\perp$ is absent. As the XY Mode degenerates into the Y Mode at zero $H_\perp$, the statements made for the Y Mode hold good for the XY Mode also when $\mathbf{H}_\perp$ is absent.

The situation becomes more complex when $\mathbf{H}_\perp$ acts in the xy plane $(\alpha \neq 0,\ \pi/2)$. The X Mode now contains ϕ as an additional distortion. While this adds to the elastic free energy, ϕ does not introduce fresh destabilizing electric torques. Hence, the X Mode threshold can be expected to rise with respect to the HD threshold as α is increased from zero. To find out whether the X Mode gets quenched, the critical condition $\delta = 0$ from (12) is studied for general α (with $\mu = 0$). This leads to a quadratic in σ_H with roots

$$\sigma_{H\pm} = \frac{-L_b \pm (L_b^2 - 4L_a L_c)^{1/2}}{2L_a};\ L_a = S_\alpha^2(\beta_3 - 1 + j(\alpha));$$

$$L_b = q^2((1-\beta_3)(1+S_\alpha^2) - 2\beta_1 S_\alpha^2);$$

$$L_c = q^4(\beta_3 + \beta_1 - 1). \tag{14}$$

Two roots $H_{C\pm}$ should result from (14). For (7), H_{C+} exists in the interval $0 < \alpha < \alpha_X$ with

$$\sin^2 \alpha_X = \frac{(1-\beta_3)^2}{(1-\beta_3)^2 + 4\beta_2(\beta_3 + \beta_1 - 1)} \tag{15}$$

and $\alpha_X \approx 1$ radian; clearly, $H_{C+} \to H_C$ of (13) when $\alpha \to 0$. In the narrow interval $\alpha_N < \alpha < \alpha_X$ with

$$\sin^2 \alpha_N = \frac{\beta_3 + \beta_2 - 1}{\beta_2 - \beta_1}, \tag{16}$$

H_{C-} also exists; $\alpha_N \approx 0.99$ radian. One can scale $H_{C\pm}$ by H_C of (13) and plot the scaled quantities as functions of α; the result is similar to the dotted curve in Figure 7a (H_{C+} and H_{C-} give the horizontal and vertical branches, respectively).

For the Y Mode, (14)–(16) can be rewritten by interchanging β_1 and β_2. Analogous to (15), one can define an angle α_Y such that the Y Mode does not exist for $\alpha > \alpha_Y$. Substitution from (7) shows that α_Y cannot be a real angle. When $\alpha = \pi/2$, ϕ gets decoupled and the Y Mode is described by θ and ψ (this holds for the XY Mode also). The reduced Y threshold $R_Y = R_0$ and wavevector $Q_{PY} = Q_0$ are given by

$$R_o = \sqrt{\beta_3(1-\beta_2)} + \sqrt{\beta_2(1-\beta_3)};$$

$$Q_o^2 = \frac{\pi^2}{4}\left(\sqrt{\frac{(1-\beta_3)(1-\beta_2)}{\beta_2\beta_3}} - 1\right); \tag{17}$$

for (7), $R_o \approx 0.97$ and $Q_o \approx 1.24$. Interestingly, this coincides exactly with the Y threshold parameters for zero magnetic field because $\mathbf{H}_\perp$ does not influence θ and ϕ damps out when $\alpha = \pi/2$. Thus, the Y Mode exists as a solution over the entire α range and $R_Y < 1$.

At general magnetic tilts, the XY Mode becomes more favourable than either the X or the Y Mode (Figs. 5a–5c). This is because the XY Mode is accompanied by the destabilizing effects of both E_x' and E_y'. Another reason is that the XY Mode is associated with additional elastic torques $(K_1 - K_2)\,\phi_{,xy}$ and $(K_1 - K_2)\,\theta_{,xy}$ that depend upon the difference in two elastic constants. Using (11), one can show [26] that these cross coupling terms have a *destabilizing* influence in the presence of elastic anisotropy. To see this, consider only the elastic terms in (4) and (5) and let θ of (11) come into existence with $\theta_A > 0$. A torque such as $\theta(\varepsilon_A E_{xo}^2/4\pi)$ in (4) has the same sign as θ_A; such a torque can be regarded as destabilizing as it encourages θ to grow and tends to destabilize $\mathbf{n}_o$. On the other hand, a torque such as $K_1\,\theta_{,xx}$ has a sign opposite to that of θ_A; such a torque can be said to be stabilizing as it tends to prevent θ from increasing. As seen from (5), the

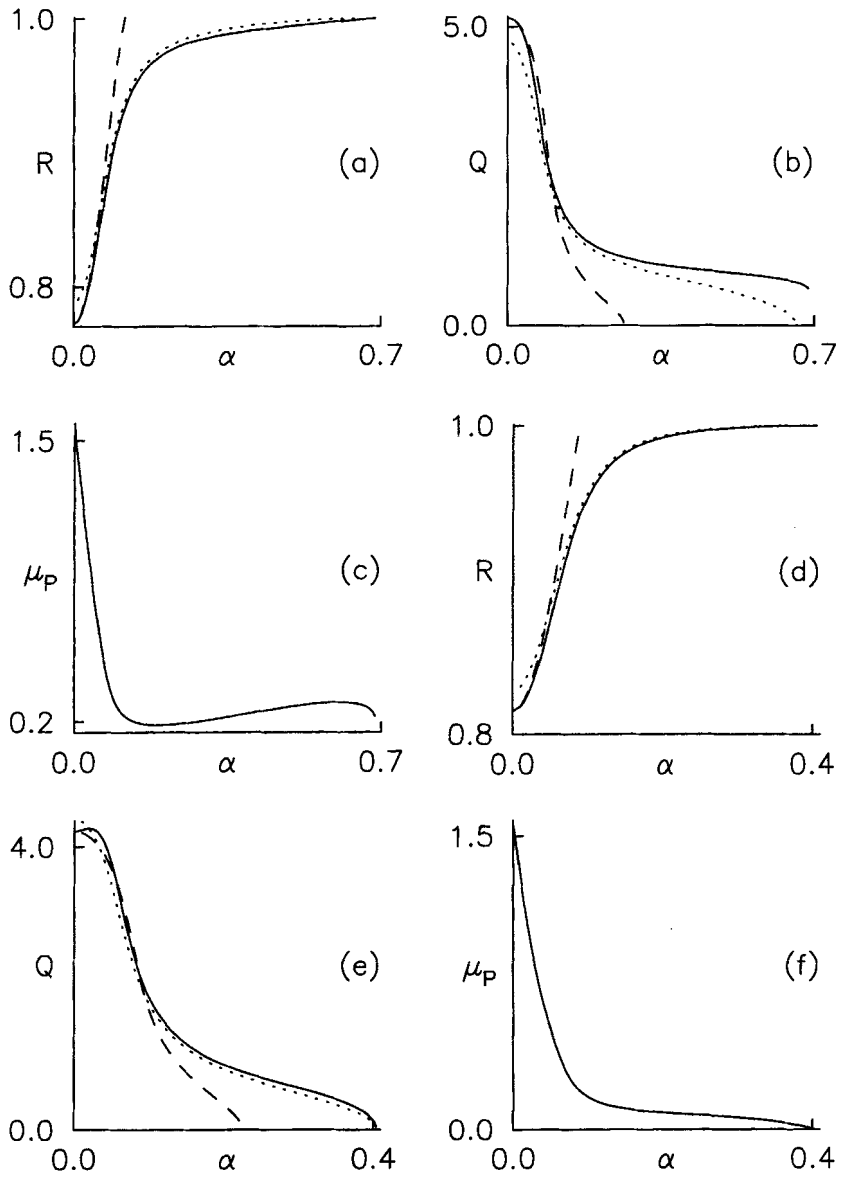

FIGURE 6 Details as in Figure 5 except that $r = 20$. $\phi_o =$ (a, b, c) 0.5 (d, e, f) 0.7 radian. In (a, b, c), the XY Mode is quenched discontinuously but its periodicity direction is closer to x than to y axis. At high enough pretilt (d, e, f), the XY Mode merges into the X Mode at a critical point (Section 4). In (a) and (d), the Y threshold curve is not represented in the range $R_Y > 1$.

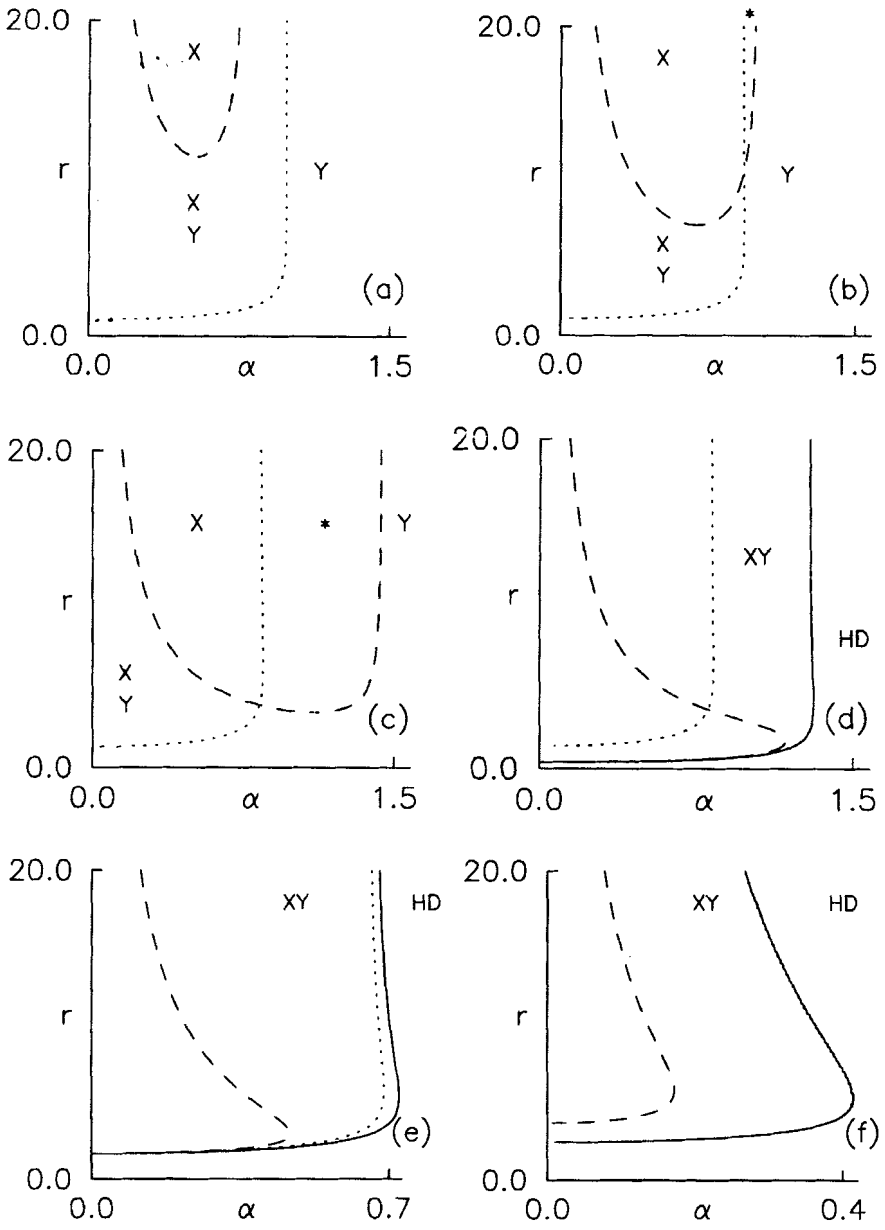

FIGURE 7 Phase diagrams in the $r - \alpha$ plane for the X (....) and Y(----) Modes at $\phi_o =$ (a) 0.1 (b) 0.2 (c) 0.32 (d) 0.34 (e) 0.5 (f) 0.8 radian. As the director pretilt is below $\phi_C = 0.328$ radian in (a)–(c), the XY Mode has lower threshold than the other deformations (including HD) over the entire region; hence, the XY phase boundary does not exist and these results are of only theoretical interest. The X and Y Modes exist in regions marked X and Y, respectively; neither Mode exists in the region *. When ϕ_o exceeds ϕ_C (d to f), the XY Mode is quenched in favour of HD and its phase boundary (—) can be drawn; in the region marked XY enclosed by —, the XY Mode is more favourable than the other deformations (see Section 4). The dotted line in (a) is similar to the X phase boundary for the homeotropic case (Section 3).

presence of elastic anisotropy causes ϕ to emerge such that

$$\phi_A = \frac{(K_2 - K_1) Q^2 S_\mu C_\mu}{(K_3 q^2 + Q^2(K_2 C_\mu^2 + K_1 S_\mu^2))} \theta_A .$$

Substituting in (4), the torque $(K_1 - K_2)\phi_{,xy}$ takes the form

$$\frac{((K_2 - K_1) Q^2 S_\mu C_\mu)^2}{(K_3 q^2 + Q^2(K_2 C_\mu^2 + K_1 S_\mu^2))} \theta_A;$$

clearly, this torque has the same sign as θ_A and is, therefore, destabilizing. When $\mathbf{H}_\perp$ is impressed away from the symmetry directions in the xy plane, the XY Mode may set in with lower threshold than even the Y or the X Mode because of the additional destabilizing torques associated with it. In the limit of $r \gg 1$, $\mu_P \to \alpha$, $R_P \to R_o$ and $Q_P \to Q_o$ of (17). Thus, the most favourable distortion is either the XY Mode (at general α) or the Y Mode ($\mathbf{H}_\perp$ acting along x or y; or, $H_\perp = 0$).

3.2. Results for Hypothetical Parameters

Before closing the discussion, two points must be elucidated. The first is a symmetry supported by the governing equations. Under interchange of K_1 and K_2, the governing equations (3)–(6) remain invariant provided that $\mu \to \mu + \pi/2$. Thus, the result of section 3.1 for the XY Mode apply exactly to a (hypothetical) material with interchanged values for the splay and twist elastic constants if the direction of periodicity is changed by $\pi/2$; in addition, results for the Y Mode (X Mode) reduce to those for the X Mode (Y Mode).

The second point concerns the effect of the elastic anisotropy $K_1 - K_2$ on the nature of the solution. In real calamitic materials, this quantity is positive and is of the order of K_2. On the other hand, a discotic nematic [20] may have $K_2 \approx 2K_1$. In addition, the discotic material has susceptibility anisotropies having the same sign as a calamitic mesogen such as CCH–7. It may be possible to prepare a nematic mixture in which the elastic difference in very small and the susceptibility anisotropies have the same sign as in (7). This makes it meaningful to consider hypothetical nematics having different levels of elastic isotropy.

Suppose $K_2 = K_1 = K_L$. For such a material, μ disappears from (12) and the function j simply takes the value β_1 or β_2. As μ does not enter the picture, $E_{xo}(Q, \mu)$ reduces to $E_{xo}(Q)$ which still depends on the magnetic tilt α.

It essence, the direction of periodicity becomes arbitrary in the xy plane and such *PD* is difficult to visualize. This illustrates the importance of elastic anisotropy in fixing the symmetry directions for studying *PD* in a homeotropic sample. We know that θ and ϕ are distortions lying in two mutually perpendicular planes containing z. The variation of θ with x and that of ϕ with y are associated with the same constant, K_1 as required by uniaxial symmetry. Similarly, $\phi_{,x}$ and $\theta_{,y}$ appear with the same constant K_2 which can be different from K_1, in general. By equating K_1 and K_2, we are making the material elastically isotropic about $\mathbf{n}_0$.

A purely formal study of $E_{xo}(Q)$ for such a material shows that the nature of the solution depends upon the magnitude of K_L with respect to K_3 if other parameters retain their values as in (7).

(a) Let $K_L/K_3 > \varepsilon_A/\varepsilon_\perp$. In such a material, H_C of (13) gives the lower cutoff field when $\mathbf{H}_\perp$ acts along x. For general magnetic tilt, *PD* cannot exist when α exceeds α_X of (15). In the range $0 < \alpha < \alpha_X$, there exist two critical fields (14) at which the *PD* is quenched and the phase diagram takes the shape of the solid line curve in Figure 7f.

(b) Let $K_L/K_3 < \varepsilon_A/\varepsilon_\perp$. For this material, neither (13) nor (15) has real solutions. Thus, *PD* exists not only for all orientations of α but also when $\mathbf{H}_\perp$ itself is absent; in the latter case, the *PD* threshold parameters are given by (17). The phase diagram cannot be drawn in the $r - \alpha$ plane.

4. EFFECT OF DIRECTOR PRETILT; $\phi_0 \neq 0$

When $\mathbf{n}_0$ is pretilted, $\mathbf{H}_\perp$ is not confined to the xy plane for general values of α. The mixed derivative terms in the governing equations (3)–(5) remain making it impossible for the perturbations to retain purity of spatial symmetry. The *ansatz* (11) has to be modified to express each perturbation as a linear superposition of two terms,

$$\theta = \theta_T(z)\sin\left(\frac{Q(x\,C_\mu + y\,S_\mu)}{h}\right) + \theta_U(z)\cos\left(\frac{Q(x\,C_\mu + y\,S_\mu)}{h}\right) \qquad (18)$$

(similarly for ϕ and ψ) where the z dependent coefficients possess definite spatial symmetry. If θ_T, ϕ_T, ψ_T possess the symmetry of SOLUTION 1, θ_U, ϕ_U, ψ_U conform to the symmetry of SOLUTION 2. Substitution of (18) in (3)–(5) yields a set of six coupled linear differential equations with z as the independent variable. These are solved numerically by the series solution

method with the boundary conditions (6) to yield a compatibility condition from which the XY threshold is computed. When μ is equated to its extreme limits, one gets the X threshold ($\mu = 0$) or the Y threshold ($\mu = \pi/2$). The dimensionless electric thresholds R_X, R_Y, R_P as well as the reduced magnetic strength r are defined as in section 3.

When (18) is substituted into (3)–(6), an additional symmetry of these equations becomes manifest with relevance to the XY Mode. This is done by comparing the equation systems written for two values of the magnetic tilt, $\alpha = \pi/2 \pm \zeta$. It is found that the two systems become identical under the transformation

$$\phi_T \rightarrow -\phi_T;\ \phi_U \rightarrow -\phi_U;\ \mu \rightarrow \mu + \pi/2.$$

This simply means that R_P and Q_P are the same for $\alpha = \pi/2 \pm \zeta$, but μ_P changes by $\pi/2$. Hence, it is sufficient to study the XY Mode in the α range $0 \leqslant \alpha \leqslant \pi/2$ even with director pretilt. This symmetry is trivially valid for the homeotropic case (see Fig. 4 of ref. 16).

Prior to a quantitative discussion of the different thresholds, some qualitative remarks seem appropriate. When ϕ_o is zero, the lowest PD threshold corresponds to the uncoupled SOLUTION 1 for any α. Once ϕ_o is increased from zero, each perturbation is represented by a 'mixture' of two terms – one from SOLUTION 1 and the other from SOLUTION 2. This superposition arises because the governing equations contain mixed derivatives as well as magnetic cross coupling terms such as $\chi_A H_\perp^2 S_z C_z \theta$. Hence, $\theta_{,yz}$ is related to θ while ϕ is related to $\phi_{,xy}$ and $\phi_{,xz}$ in (4); similarly, $\phi_{,yz}$ is related to ϕ while θ is related to $\theta_{,xy}$ and $\theta_{,xz}$ in (5). Suppose α is fixed. Then, greater the deviation of ϕ_o from zero, higher the component of the less favourable SOLUTION 2. But HD continues to be described by a solution with pure spatial symmetry. Naturally, the PD threshold rises with respect to the HD threshold when ϕ_o is increased from zero. When ϕ_o exceeds some limiting value, PD may become less favourable than HD. The critical ϕ_o at which PD is quenched will depend upon the PD Mode under study. In the same way, one can expect a critical α value (at a fixed ϕ_o) at which PD may get quenched.

The next question is, how does the PD wavevector behave when PD is suppressed? This question can be answered by a look at the boundary conditions (6). Clearly, the X Mode and HD share the same set of boundary conditions. Naively, one can expect a critical point between the two; when the X Mode and HD thresholds become equal, Q_{PX} should vanish. This is actually borne out by explicit computation but is difficult to establish analytically

for general values of the geometric parameters. The special case $\alpha = 0$ is, however, simple. The X Mode can now be described by two uncoupled solutions:

SOLUTION A: θ is even; ψ and ϕ are odd;
SOLUTION B: θ is odd; ψ and ϕ are even.

SOLUTION A is an extension of HD with threshold (10) except that HD is not associated with ϕ at $\alpha = 0$. A critical point will exist between the X Mode and HD if ϕ and Q_{PX} vanish in the same limit. This can be proved to hold and the critical condition derived using the approach of ref. 27. The *ansatz* (18) is substituted in (3)–(6) and each perturbation is expanded in powers of Q (with the prior assumption that μ and α vanish). The governing equations are now solved for SOLUTION A. Substituting in (2) and integrating over the sample volume, the total free energy can be written (upto lowest power in Q) as $N_o + Q^2 N_1$ where N_o is the aperiodic (or HD) term. If $N_1 < 0$, the X Mode (SOLUTION A) is more favourable than HD; $N_1 = 0$ yields the critical point between the X Mode and HD,

$$H_A^2(\phi_o) = \frac{\pi^2 f_3}{4h^2 \varepsilon_A \chi_A C^2}\left(\frac{\varepsilon_A C^2 f_1}{f_3} + \frac{(K_1 - K_2)^2 S^2}{f_2} - K_1\right)$$

with $C \neq 0$. Clearly, $H_A(0) = H_C$ of (13).

On the other hand, the Y Mode boundary conditions are different from those of HD regardless of the magnetic tilt (observe the term containing $\psi_{,y}$ in eqn. 6). Hence, the Y Mode and HD cannot share a critical point (when the Y Mode and HD thresholds become equal, $Q_{PY} \neq 0$. in general). The discussion for the XY Mode is not straightforward even though, apparently, it has the same set of boundary conditions as the Y Mode. As the X and Y Modes are but limits of the XY Mode at two extreme values of μ (corresponding to two symmetry directions in the sample), we have to consider not only Q_P but also μ_P when the XY Mode and HD thresholds become equal. There are three possibilities when $R_P = 1$:

(i) $Q_P = 0$ and $\mu_P = 0$. This would correspond to the XY Mode merging into HD by turning into the X Mode. With respect to the order parameter Q_P, this transition is one of second order.
(ii) $Q_P \neq 0$ and $\mu_P = \pi/2$; then, the XY Mode approaches HD via the Y Mode. The transition is one of first order; calculations show that this occurs generally when ϕ_o is small.

(iii) $Q_P \neq 0$ and $\mu_P \neq 0$ or $\pi/2$. This transition is discontinuous; this appears to hold whenever the XY and Y phase boundaries lie close to each other.

Even though the XY Mode is found to be the most favourable of the three *PD* Modes, results have been presented for all Modes; this helps in visualizing the results especially where the XY Mode merges into one of the remaining *PD* Modes before getting damped.

4.1. Results for Real Parameters

Initial results (Figs. 1 and 2) depict the variation of threshold parameters with the stabilizing magnetic field (or, equivalently, r) for a real material (7). For simplicity, we restrict r to the range $0 \leqslant r \leqslant 20$. When α and ϕ_0 are small (Figs. 1a–1c; the director pretilt is almost zero and $\mathbf{H}_\perp$ acts close to the x axis), the X Mode is uniformly unfavourable over the entire r range and exhibits a critical point close to $r = 1$. The thresholds and wavevectors of the Y and XY Modes almost overlap; these Modes also exist over the entire r range showing that *HD* cannot set in even in the absence of $\mathbf{H}_\perp$. The angle between the XY Mode wavevector and x axis (μ_P) decreases with increase of r but is close to $\pi/2$ at $r = 0$ (where the XY Mode degenerates into the Y Mode) (Fig. 1c); in this limit, $R_P \to R_o$ and $Q_P \to Q_o$ of (17). At high enough r, μ_P should approach α; such high values of r have not been considered here.

When the magnetic tilt is increased (Figs. 1d–1f; $\alpha = 0.3$), other features of the instabilities manifest. Again, the XY Mode has the lowest threshold over the entire r range and *HD* cannot occur even at zero r. To be noted, however, is the marked decrease of μ_P from $\pi/2$ at $r = 0$ to a value close to α when $\mathbf{H}_\perp$ is strong enough; in this limit, the XY threshold approaches the X threshold. The shapes of the R and Q curves are completely different from those of Figures 1a–1c; while R shows a minimum, Q exhibits a maximum when r is increased from zero. The Y Mode is quenched at strong $\mathbf{H}_\perp$ via a critical point with *HD*. The results for the XY Mode are close to those obtained earlier (see Figs. 4a–4c of ref. 16).

When the director pretilt is high (Fig. 2), the XY Mode continues to have lower threshold than the X and Y Modes over its range of existence. When α is small (Figs. 2a–2c), the XY Mode is close to the Y Mode at high r. On lowering r, the XY threshold parameters exhibit a discontinuous change when the cross over occurs from the Y to the X mode (Figs. 2b, 2c). The XY Mode gets quenched when r is lowered further; the critical point (r_C) is identical to that of the X Mode. For $0 < r < r_C$, only *HD* should

set in. Though the Y Mode exists as a solution down to $r = 0$, it is of no real interest as $R_Y > 1$. When $\mathbf{H}_\perp$ is rotated away from the x axis (Figs. 2d–2f), the XY Mode is found to be close to the X Mode over its range of existence and exhibits two critical points $0 < r_1 < r_2$; the X Mode also gets quenched at the same points. In this case, HD exists in the ranges $0 < r < r_1$ and $r > r_2$.

The different ways in which the XY Mode behaves with r variation should also manifest when other parameters are varied. In a real situation, the director pretilt cannot be changed continuously. Different pretilts may be imparted by different surface treatments to the sample boundaries. This will also imply different director anchoring strengths. In this work, the rigid anchoring hypothesis has been assumed. Hence, the ϕ_o variation is treated as a purely theoretical calculation related to the change in one of the independent parameters. Figures 3 and 4 depict the effect of varying ϕ_o at fixed $\mathbf{H}_\perp$. As expected, the XY Mode meets HD in a critical point when ϕ_o is sufficiently high. The XY Mode is close to the Y Mode (or X Mode) at low (or high) ϕ_o. In particular, the XY Mode merges with the X Mode at the critical point. However, the nature of variation of the threshold parameters is different at different r and α.

When $\mathbf{H}_\perp$ is close to the x axis and r high enough (Figs. 3a–3c), the XY Mode crosses over from the Y to the X Mode smoothly; this is because the X and Y Mode threshold parameters are close to one another over the entire ϕ_o range. When $\mathbf{H}_\perp$ is not strong enough (Figs. 3d–3f), the crossover occurs discontinuously; this is similar to the behaviour seen in Figures 2a–2c. When $\mathbf{H}_\perp$ is rotated away from the x axis (Figs. 4a–4c), the discontinuity disappears even at low r. At sufficiently high α, the X Modes does not exists even as a solution (Figs. 4d–4f). When ϕ_o is raised, R_p increases beyond unity before ceasing to exist; when $R_p = 1$, Q_p is non-zero and μ_p does not take either of its limiting values.

It is clear from Figures 3 and 4 that the ϕ_o range of existence of the Y Mode is shorter than that of the X Mode. This can be explained qualitatively as follows. The principal stabilizing torques associated with the x periodicity are $K_1\theta_{,xx}$ and $K_2\phi_{,xx}$; these are independent of ϕ_o. On the other hand, the corresponding torques associated with the Y Mode are $(K_2C^2 + K_3S^2)\theta_{,yy}$ and $(K_1C^2 + K_3S^2)\phi_{,yy}$; both these stabilizing torques get stronger with increase of ϕ_o. Though the thresholds of both the Modes increase with the director pretilt (at given r and α), the above reason may lead to a crossover by causing the Y threshold to exceed the X threshold above some limiting ϕ_o.

As found in Section 3, only the Y Mode exists when $\mathbf{H}_\perp$ is absent and $\mathbf{n}_0$ is homeotropic. If the director pretilt is now increased, the Y threshold increases relative to the HD threshold due to the increasing addition of SOLUTION 2 to SOLUTION 1. At a critical $\phi_o = \phi_C$, $R_p = 1$ showing that for $\phi_o > \phi_C$, HD sets in. For the parameters (7), $\phi_C \approx 0.328$ radian; at this point; Q_{PY} is non-zero. As the XY Mode degenerates into the Y Mode when $r = 0$, ϕ_C also happens to be quenching point for the XY Mode. The significance of this quantity emerges from detailed calculations for different r and α; it is found that as long as $0 < \phi_o < \phi_C$, the XY Mode exists and is more favourable than the X and the Y Modes in the presence of a stabilizing $\mathbf{H}_\perp$.

The variation of α at given r and ϕ_o complements the previous results. The XY Mode exists as a solution over the entire α range $0 \leqslant \alpha \leqslant \pi/2$ (Fig. 5) as long as the director predtilt is not very high. The results for $\pi/2 \leqslant \alpha \leqslant \pi$ can be obtained from these curves by suitable reflections in the axes following the invariance transformation discussed above. The curves are initially reflected in the vertical line $\alpha = \pi/2$. In the case of the μ_P curves, a further reflection in the horizontal line $\mu_P = \pi/2$ is needed. When $\mathbf{n}_0$ is close to the homeotropic, (Figs. 5a–5c), the XY Mode is the most favourable distortion over the entire α range; at $\alpha = 0, \pi/2$, the XY Mode is close to the Y Mode. When the director pretilt is higher (Figs. 5d–5f), this behaviour continues but the XY threshold exceeds the HD threshold when the magnetic tilt is sufficiently high. The transition between the XY Mode and HD is discontinuous in this case but the XY Mode periodicity direction is closer to the y axis than to the x axis (Fig. 5f). Further increase of director pretilt (Figs. 6a–6c) again shows a discontinuous quenching of the XY Mode in favour of HD; but now the direction of the XY Mode periodicity is closer to x than to y; in addition, the XY Mode does not exist as a solution over the entire α range. When $\mathbf{n}_0$ is pretilted well away from the homeotropic (Figs. 6d– 6f), the XY Mode merges into the X Mode before being damped out at the critical point.

It is now possible to visualize the phase diagrams. The first set (Fig. 7) are related to α variation at constant ϕ_o. To get the phase boundary separating the XY Mode and HD, r is initially fixed at a high value. Starting with $\mathbf{H}_\perp$ close to the x axis, α is increased in small steps; for each value of α, R_P, Q_P and μ_P are determined. When $\phi_o > \phi_C$, $R_P \to 1$ when $\alpha \to \alpha_C$; at this point, the value of Q_p determines whether the transition is of second or first order. The values of μ_P at $\alpha = \alpha_C$ determines whether the XY Mode is close to the X Mode or the Y Mode. This is repeated for different values of r. The plot of r versus α_C yields the phase boundary between the XY Mode and HD. In a

similar way, the phase boundaries for the X and Y Modes are determined by much simpler computation.

When $\phi_o < \phi_C$, the XY Mode exists at all α (atleast over the range of r studied in this work); hence, the phase boundary for the XY Mode is non-existent. In addition, the XY Mode has lower threshold than either the X or the Y Mode. Yet, results (of purely academic interest) are presented in this ϕ_o range for the X and Y Modes (Figs. 7a–7c) to understand how their phase boundaries alter in shape as the pretilt of $\mathbf{n}_0$ is increased from the homeotropic. It is known (Section 3) that the Y Mode exists as a solution with $R_Y < 1$ for all α when $\mathbf{n}_0$ is homeotropic. Hence, at $\phi_o = 0$, the Y phase boundary is non-existent; only the X mode can be represented.

But even at low director pretilt (Fig. 7a), the Y Mode is quenched when α is changed away from either edge of its range; as remarked already, Q_{PY} is non-zero on the phase boundary. For the X Mode, however, the dotted line represents a critical boundary; when $R_X \to 1$, $Q_{PX} \to 0$. It is seen that the Y Mode is favourable at low r and also near $\alpha = \pi/2$. The X Mode alone exists over a narrow α range when r is high enough. For lower values of r, both the X and the Y Modes exist as solutions; here, explicit computation of R_X and R_Y will decide which Mode is the more favourable. It may be stated intuitively that the Y Mode (or the X Mode) is more favourable at a point close to the dotted (or the dashed) line. An increase of ϕ_o (Fig. 7b) causes a narrowing of the α ranges of existence of both the X and the Y Modes; in addition, a new portion of the diagram (*) emerges where the X Mode does not exist and the Y threshold exceeds that of HD. Close to $\phi_o = \phi_C$ (Fig. 7c), the region (*) becomes greatly expanded.

This indicates the possible shapes of the different phase boundaries when ϕ_o is increased beyond ϕ_C (Figs. 7d–7f). Now, the XY Mode can be quenched by increasing α above a certain limit; the XY Mode does not exist near the upper end of the α range. In general, HD is more favourable when r is small or when $\mathbf{H}_\perp$ acts close to the yz plane. When ϕ_o is close to ϕ_C (Fig. 7d), the XY Mode boundary never comes close to the X Mode periphery. In the low r range, the XY Mode merges with the Y Mode while getting quenched. Hence, the change from the XY Mode to HD is discontinuous (Q_P is non-zero). At a higher ϕ_o (Fig. 7e), the XY and X Mode come close to each other at elevated r values; here, the discontinuity in the transition between the XY Mode and HD is much reduced. When the director pretilt is high enough (Fig. 7f), the XY Mode and X Mode peripheries coincide; the Y phase boundary is completely enclosed by the XY (or X) boundary. The XY Mode merges with the X Mode on the quenching line so that when $R_P \to 1$ and Q_P, $\mu_P \to 0$.

The phase boundaries in the $r-\phi_o$ plane are obtained by a procedure similar to the one employed to draw (Fig. 7). In this case, ϕ_o is varied at fixed r and α. The phase plane is again divident into two parts – XY and HD – corresponding to the occurrence of the XY Mode and HD. At given r and α, the XY Mode gets quenched with increase of director pretilt. Increase of magnetic tilt causes the domain of existence of the XY Mode to shrink. In all diagrams, the intercept of the XY boundary with the ϕ_o axis is ϕ_C. When $\mathbf{H}_\perp$ acts close to the x axis (Fig. 8a), the XY phase boundary merges into that of the X Mode (or the Y Mode) in the high (or low) r range; the change over occurs sharply (see the horizontal line). Increase of α causes the change over to occur at higher r; the width of discontinuity also diminishes (Figs. 8b, 8c). At sufficiently high α (Figs. 8d, 8e), the X phase boundary gets separated from that of the XY Mode. The approach of the XY and Y phase boundaries is not separated by a discontinuity. When $\mathbf{H}_\perp$ acts close to the yz plane (Fig. 8f), the X Mode does not exist as a solution but the XY and Y boundaries lie close to each other.

4.2. Hypothetical Materials

Before closing; it seems appropriate to comment on the hypothetical materials having elastic isotropy about $\mathbf{n}_0$ ($K_1 = K_2 = K_L$) in the context of director pretilt. When $\phi_o \neq 0$, the cylindrical symmetry about z is destroyed. This manifests itself in the form of different boundary conditions for different deformations. As the elastic torques depending upon $K_1 - K_2$ no longer appear, the XY Mode does not exist as a solution with arbitrary μ_p regardless of the value of K_L; it reduces to the X Mode ($\mu_P \to 0$) or to the Y Mode ($\mu_P \to \pi/2$). Due to the reason given in Section 4.1, the X Mode is found to be always more favourable than the Y Mode. This also means that under the variation of a given geometric factor, the X Mode continues to exist at a point where the Y Modes gets quenched. In every case, the Y phase boundary is completely enclosed by the X Phase boundary. The shapes of the Phase boundaries, however, depend upon the relative values of K_L and K_3.

The solution for the Y Mode remains analytically intractable due to the mixing of SOLUTIONs 1 and 2. But simplification is discernible in the case of the X Mode. The mixed derivatives $\theta_{,xz}$ and $\phi_{,xz}$ having dropped out of the governing equations, the X Mode degenerates into the two uncoupled SOLUTIONs 1 and 2 of which SOLUTION 1 is studied as it is an extension of HD. The X Mode threshold and phase boundary can be found analytically using the *ansatz* (11) with $\mu = 0$. The expression for $E_{xo}(Q)$ is

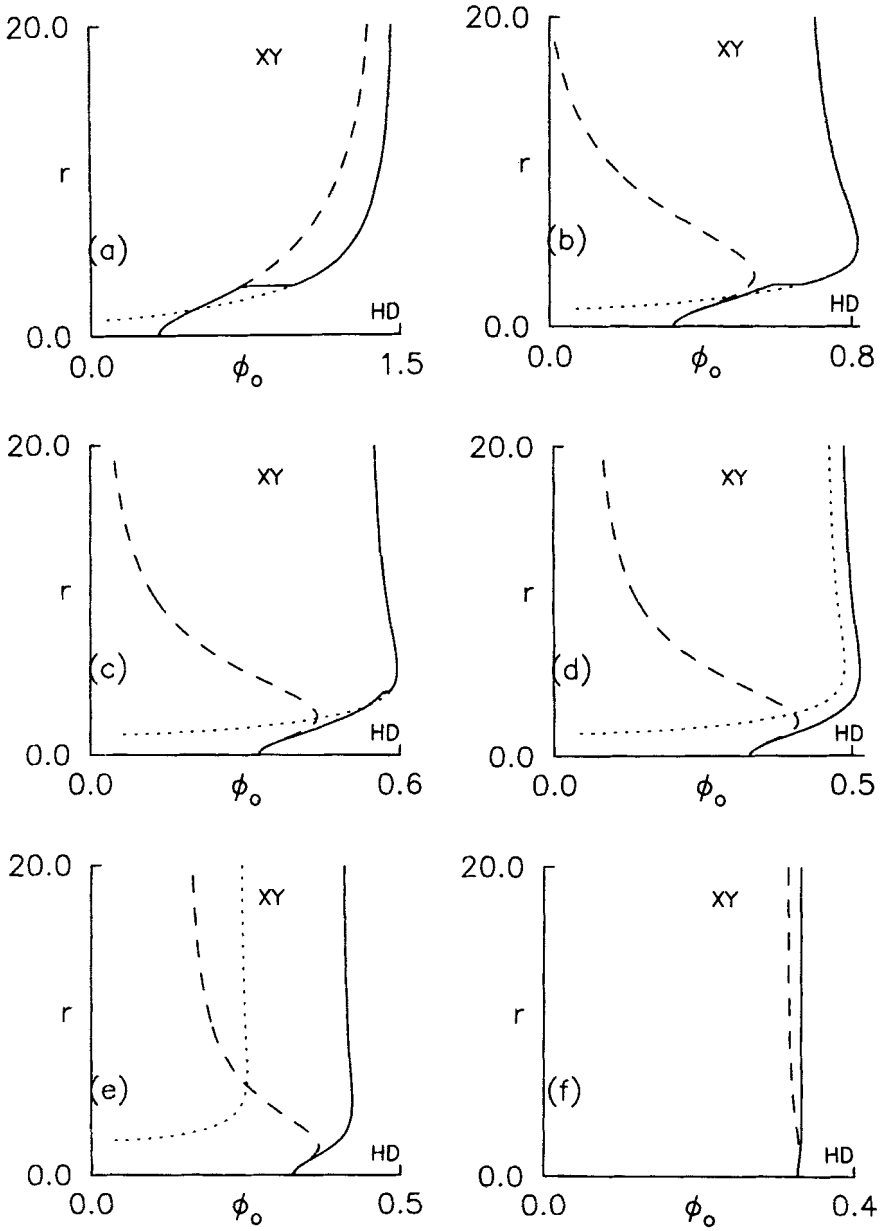

FIGURE 8 Phase diagram in the $r - \phi_o$ plane for the X (....), Y(----) and XY(——) Modes at different magnetic tilts; α = (a) 0.01 (b) 0.4 (c) 0.6 (d) 0.7 (e) 0.9 (f) 1.4 radian. The XY Mode exists in the region marked XY enclosed by (—). The discontinuity in the XY phase boundary is noticeable (a–c) when $\mathbf{H}_\perp$ acts sufficiently close to the x axis (see Figs. 2a–2c, 3d–3f). At higher α (f), the X phase boundary itself is absent (Section 4).

identical to (12) except that the coefficients are redefined:

$$t_1 = \gamma_2 \gamma_1^2;\ u_1 = \gamma_1;\ t_4 = q^4\left(q^2 - \frac{\chi_A h^2 H_\perp{}^2}{f_2}\right);$$

$$t_2 = \gamma_1 q^2(\gamma_1 + \gamma_2) + t_4\frac{\gamma_1\gamma_2}{q^4};\ u_3 = q^2\sigma_E;$$

$$t_3 = q^4\gamma_1 + t_4\frac{(\gamma_1 + \gamma_2)}{q^2};\ u_2 = \gamma_1 q^2 + \sigma_E;$$

$$\gamma_1 = \frac{K_L}{f_2};\ \gamma_2 = \frac{\varepsilon_\perp}{f_3};\ f_2 = f_1 = K_3 C^2 + K_L S^2. \tag{19}$$

where $q = \pi/2$ (see also Eqn. 10). When Q is small, the critical condition $t_3 u_3 - t_4 u_2 = 0$ leads to a quadratic

$$(\sigma_B^2 S_\alpha^2 + q^4)(\gamma_1 + \gamma_2 - 1) + \sigma_B q^2(1 - \gamma_2 + S_\alpha^2(1 - \gamma_2 - 2\gamma_1)) = 0;$$

$$\sigma_B = \frac{\chi_A h^2 H_\perp{}^2}{f_2}, \tag{20}$$

which shows that at general α there may exist two critical points between the X Mode and HD; conclusions (21)–(23) also follow and their significance is determined by the relative magnitudes of the material parameters.

(i) If $\mathbf{H}_\perp$ is not impressed, (20) leads to the definition of a critical director pretilt, $\phi_o = \phi_X$

$$\cos^4\phi_X = \frac{K_L\varepsilon_\perp}{(K_3 - K_L)\varepsilon_A} \tag{21}$$

(ii) At a given ϕ_o, (20) cannot possess real roots if $\alpha > \alpha_B$ where

$$\sin\alpha_B = \frac{1 - \gamma_2}{2\gamma_1 + \gamma_2 - 1} \tag{22}$$

provided that α_B exists. Interestingly, α_X of (15) reduces exactly to α_B of (22) under the assumption $\beta_1 = \beta_2$ valid in this section.

(iii) At a given magnetic tilt, (20) cannot possess real roots if $\phi_o > \phi_B$ where

$$\cos^2\phi_B = \frac{-L_2 + \sqrt{L_2^2 + 4L_1L_3}}{2L_1};\ L_1 = (K_3 - K_L)\varepsilon_A(1 + S_\alpha);$$

$$L_2 = K_L\varepsilon_A(1 - S_\alpha);\ L_3 = 2K_L\varepsilon_\perp S_\alpha \tag{23}$$

if ϕ_B exists. The interpretation of (21)–(23) can be done under two different heads. As these are derived from the same expression (20), they are found to be self-consistent.

a. Let $K_L/K_3 > \varepsilon_A/\varepsilon_\perp$. In such a material, ϕ_X of (21) is not real but H_C of (13) exists. Then, the X threshold exists only in the presence of a sufficiently strong $\mathbf{H}_\perp$. At a given α, the X Mode has two cut off points given by (20) provided that the director pretilt is not too high ($0 < \phi_o < \phi_B$). Similarly, the X Mode exists between two critical magnetic strengths (20) if the magnetic tilt is not very high ($0 < \alpha < \alpha_B$). The phase diagrams for the X Mode will have the typical shape of the solid line curve of Figure 7f for both the α and the ϕ_o variations.

b. Let $K_L/K_3 < \varepsilon_A/\varepsilon_\perp$. The main conclusions of (a) are all valid except that ϕ_X of (21) exists. It is found that for $\phi_o < \phi_X$, a critical point between the X Mode and HD does not exist; i.e., the X Mode cannot be quenched for any α and any r. In particular, the X Mode exists even in the absence of $\mathbf{H}_\perp$. At $\phi_o \geqslant \phi_X$, $\alpha_B \leqslant \pi/2$ (see eqn. (22)); then the X Mode can be damped out by varying the magnetic tilt. As H_C (13) does not exist, a convenient reference field can be used to measure $\mathbf{H}_\perp$ for defining the dimensionless magnetic strength r and for drawing the phase diagrams. Clearly, the X boundary in the $r - \alpha$ plane has the shape of the solid line curve in Figure 7f if $\phi_o > \phi_X$ (eqn. (21)). On the other hand, the X boundary in the $r - \phi_o$ plane extends right down to $r = 0$ where it intersects the ϕ_o axis at $\phi_o = \phi_X$; the general shape of the X boundary is that of the dashed curves in Figures 8a or 8d, depending upon the magnetic tilt.

5. CONCLUSIONS

A nematic with parameters (7) is uniformly aligned in the yz plane at a director pretilt ϕ_o with respect to z and subjected to the actions of $\mathbf{E}_0$ along x and $\mathbf{H}_\perp$ in a plane normal to $\mathbf{n}_0$. The stability of the initial orientation is studied by linear perturbation analysis. In general, director perturbations

are accompanied by a perturbation in the electric potential. A deformation is induced by the electric field under the stabilizing influence of $\mathbf{H}_\perp$. When $\mathbf{n}_0$ is homeotropic, *PD* is more favourable than *HD* for any magnetic strength or magnetic orientation in the xy plane; this is the result of additional destabilizing torques that are associated with periodic perturbations. *PD* in this case is described by perturbations with pure spatial symmetry with respect to z (SOLUTION 1). In addition, *PD* and *HD* have the same set of boundary conditions. Due to the elastic anisotropy $K_1 - K_2$, the direction of periodicity varies in the xy plane with changing magnetic tilt α. When $\mathbf{H}_\perp$ is absent or when $\mathbf{H}_\perp$ acts along the symmetry directions, the periodicity is along y. In a hypothetical material having equal K_1 and K_2, a unique direction of periodicity in the xy plane cannot be defined.

When $\mathbf{n}_0$ is pretilted away from the homeotropic in the yz plane, the nature of *PD* changes perceptibly for parameters (7). This is mainly because each periodic perturbation is now represented by a linear superposition of two terms having opposite spatial symmetry. The addition of the less favourable component tends to increase the total free energy of *PD* relative to that of *HD* so that the *PD* threshold may exceed the *HD* threshold over a range of director pretilts, magnetic angles and magnetic strengths. In general, the boundary conditions for *PD* and *HD* are different; they become identical only when the direction of periodicity is along x. If the periodicity is along x when *PD* gets extinguished, then *PD* and *HD* meet in a critical point (the wavevector amplitude becomes zero). The wavevector is non-zero when the *PD* and *HD* thresholds become equal if the direction of periodicity happens to lie away from x.

In the absence of $\mathbf{H}_\perp$, *PD* has periodicity along y and can be quenched discontinuously if ϕ_o is higher than a critical value, ϕ_C. With a stabilizing $\mathbf{H}_\perp$, the ϕ_o range of existence of *PD* is increased (Figs. 3 and 4). When *PD* ceases to exist at sufficiently high director pretilts, the direction of periodicity is generally along x. In general, *PD* is more favourable than *HD* for $\phi_o < \phi_C$ and in the limit of weak $\mathbf{H}_\perp$, the direction of periodicity is along y (Fig. 1). When $\phi_o > \phi_C$, *PD* is damped out by reducing $\mathbf{H}_\perp$ below a critical value (Fig. 2); at the critical point, the periodicity direction is along x. The tilting of $\mathbf{H}_\perp$ sufficiently away from $\mathbf{E}_0$ can raise the *PD* threshold above the *HD* threshold provided that $\phi_o > \phi_C$ (Figs. 5d–5f and 6); in this case, however, the transition from *PD* to *HD* occurs discontinuously with respect to the wavevector. Phase diagrams drawn in different planes of the parameter space (Figs. 7d–7f and 8) indicate not only the range of existence of *PD* but also its periodicity direction while damping out. It is found, for instance, that *PD* can be quenched at two values of $\mathbf{H}_\perp$ when ϕ_o and α are high

enough (Fig. 7f). The *PD* threshold parameters undergo a discontinuous change (Figs. 2a–2c) with a variation of $H_\perp$ when ϕ_o is high; a similar jump is evident when ϕ_o is varied at constant $H_\perp$ (Figs. 3d–3f). In both these cases, $H_\perp$ is impressed close to x axis. This discontinuity manifests itself in some of the phase diagrams involving the variation of director pretilt (Figs. 8a–8c). The discontinuity generally disappears if the magnetic tilt is sufficiently high (Figs. 2d–2f, 4a–4c, 8d–8f).

The study is extended to a hypothetical material with equal splay and twist constants. The x and y symmetry directions can be distinguished due to the director pretilt in the yz plane. The most favourable form of *PD* now occurs with periodicity along x and is described SOLUTION 1. Expressions for *PD* threshold and critical points can be analytically obtained. This makes possible a clearer visualization of some of the results obtained for real parameters – for instance, existence of cut-off values of magnetic tilt and director pretilt, two critical magnetic fields at general magnetic tilt, etc.

The results have been obtained with the linear perturbation hypothesis so that the threshold condition does not explicitly involve the actual perturbation amplitudes. The calculations are strictly valid at threshold and the variation of quantities above threshold cannot be predicted. The different non-linear phenomena that can arise are similar to those described in Section 5 of ref. 19 The boundary conditions (6) enable a closed solution to be obtained for the governing equations (3)–(5) but the continuity of tangential components of **E** at the sample boundaries is not explicitly imposed. Flexoelectricity is ignored and the director assumed to be rigidly anchored at the boundaries. This makes it meaningful to believe that the uniformly aligned ground state remains undistored upto the linear threshold. It is well known [28] that in the presence of flexoelectricity and weak anchoring, the ground state may undergo a thresholdless distortion. Hence, the results may not be physically meaningful if the applied voltage does not have a sufficiently high frequency.

In the main, parameters (7) have been considered. The results may also hold qualitatively for a nematics having similar material parameters. This does not, however, apply to the discotic studied in ref. 20 as this substance has a very high twist constant. The calculations involving continuous variation of director pretilt (Figs. 3, 4 and 8) have been included for completeness though they may not be relevant from the experiment viewpoint. As the calculations are also computer intensive, all aspects of ϕ_o variation have not been investigated in detail (for instance, the discontinuity in Figs. 8a–8c).

The material is assumed to be an insulator in this work. Hence, the presence of free charge has been ignored in (3). Real nematics generally possess ionic impurities. The effect of $\mathbf{E}_0$ applied parallel to the sample plane has been recently studied [29–31] with commercially available 5*CB*. For homeotropic $\mathbf{n}_0$, the effects of electrical conductivity are apparent in the form of frequency dependence of distortion thresholds. At low frequencies, even electrohydrodynamic effects have been observed. The electrode gap ($2g$) is assumed to be large compared to the sample thickness ($2h$). Hence, boundary conditions have not been imposed at the electrode surfaces and the x dependence has been taken to be sinusoidal. The ground state is assumed to be uniformly aligned throughout the sample. This also leads to the conclusion that at threshold, the distortion sets in over the entire sample at the same time. In experiments [29–31], the electrode gap is a small multiple of the sample thickness. Hence, the above simplification in the mathematical model may turn out to be drastic.

This work utilizes the non-stochastic continuum theory. The perturbations are imposed on $\mathbf{n}_0$ and $\mathbf{E}_0$ but driving terms for the perturbations are not included in (4) and (5). The occurrence of pretransitional biaxiality in 5*CB* [13] demonstrates the importance of explicitly including the thermal terms in the governing equations. Recent experiments show [31] that thermal fluctuations actually lead to a select build up of distortion near the electrodes (probably aided by defects that may exist near the edges between the sample planes and electrodes). Thus, a realistic model may have to incorporate thermal fluctuations as well as the possibility of a deformed ground state. From the experiment viewpoint, however, a homeotropically aligned sample of $CCH-7$ presents a novel geometry for studying the effect of a stabilizing magnetic field on pretransitional biaxiality.

References

[1] P. G. de Gennes and J. Prost, *The Physics of Liquid Crystals*, Clarendon Press, Oxford (1993).
[2] S. Chandrasekhar, *Liquid Crystals*, Cambridge University Press (1992).
[3] L. M. Blinov and V. G. Chigrinov, *Electrooptic Effects in Liquid Crystal Materials*, Springer Verlag (1993).
[4] S. A. Pikin, *Structural Transformations in Liquid Crystals*, Gordon and Breach (1991).
[5] F. Lonberg and R. B. Meyer, *Phys. Rev. Lett.*, **55**, 718 (1985); U. D. Kini, *J. Phys. France* **47**, 693 (1986); W. Zimmermann and L. Kramer, *Phys. Rev. Lett.*, **56**, 2655 (1986); C. Oldano, *Phys. Rev. Lett.*, **56**, 1098 (1986).
[6] H. J. Deuling, *Solid State Physics Supplement*, **14**, 77 (1978).
[7] R. B. Meyer, *Phys. Rev. Lett.*, **22**, 918 (1969).
[8] L. K. Vistin, *Sov. Phys. Crystallogr.*, **15**, 514 (1970); Yu. P. Bobylev, V. G. Chigrinov and S. A. Pikin, *J. Phys. Colloq. France*, **40**, C3-331 (1979).

[9] W. H. De Jeu, C. J. Gerritsma, P. Van Zanten and W. J. A. Goossens, *Phys. Lett.*, **39A**, 335 (1972); M. I. Barnik, L. M. Blinov, A. N. Trifanov, V. G. Chigrinov and T. V. Korishko, *Zh. Eksp. Teor. Fiz.*, **87**, 196 (1984).
[10] C. Gooden, R. Mahmood, A. Brisbin, A. Baldwin, D. L. Johnson and M. E. Neubert, *Phys. Rev. Lett.*, **54**, 1035 (1985); D. W. Allender, R. M. Hornreich and D. L. Johnson, *Phys. Rev. Lett.*, **59**, 2654 (1987); U. D. Kini, *Liquid Crystals*, **7**, 185 (1990).
[11] G. Srajer, F. Lonberg and R. B. Meyer, *Phys. Rev. Lett.*, **67**, 1102 (1991).
[12] S. M. Arakelyan, A. S. Karayan and Y. S. Chilingaryan, *Soviet Physics Doklady*, **29**, 202 (1984); B. J. Frisken and P. Palffy-Muhoray, *Phys. Rev.*, **A39**, 1513 (1989); *ibid*, **40**, 6099 (1989).
[13] B. J. Frisken and O. Palffy-Muhoray, *Liquid Crystals*, **5**, 623 (1989).
[14] D. W. Allender, B. J. Frisken and P. Palffy-Muhoray, *Liquid Crystals*, **5**, 735 (1989).
[15] U. D. Kini, *J. Phys. France*, **51**, 529 (1990).
[16] U. D. Kini, *J. Phys. France*, **II 5**, 1841 (1995).
[17] Hp. Schad and S. M. Kelly, *Mol. Cryst. Liquid Cryst.*, **133**, 75 (1986).
[18] Hp. Schad and M. A. Osman, *J. Chem. Phys.*, **75**, 880 (1981).
[19] U. D. Kini, *Mol. Cryst. Liquid Cryst.*, **289**, 181 (1996).
[20] T. Othman, M. Gharbia, A. Gharbi, C. Destrade and G. Durand, *Liq. Cryst.*, **18**, 839 (1995); T. Othman, M. M. Jebari, A. Gharbi and G. Durand, *Molec. Cryst. Liquid Cryst.*, **281**, 145 (1996).
[21] T. J. Phillips, V. Minter and J. C. Jones, *Liq. Cryst.*, **21**, 581 (1996).
[22] A. Rapini and M. Papoular, *J. Phys. Colloq. France*, **30**, C4-54, (1969); for reviews on interfacial effects, see J. Cognard, *Mol. Cryst. Liquid Cryst. Suppl.*, **1**, 1 (1982) and B. Jerome, *Rep. Progr. Phys.*, **54**, 391 (1991).
[23] E. Miraldi, C. Oldano and A. Strigazzi, *Phys. Rev.*, **A34**, 4348 (1986); U. D. Kini, *J. Phys. France*, **47**, 1829 (1986); *Liq. Cryst.*, **21**, 713 (1996).
[24] L. D. Landau and E. M. Lifshitz, *Electrodynamics of Continuous Media*, Pergamon Press, (1984).
[25] In ref. 16, *X*, *Y* and *XY* Modes are referred to as *xz*, *yz* and *xyz* Modes, respectively.
[26] U. D. Kini, *Molec. Cryst. Liquid Cryst.*, **153**, 1 (1987); this work employs the language of torques to show how *PD* may be more favourable than *HD* in materials with high elastic anisotropy (see also ref. 5 above).
[27] G. Cohen and R. M. Hornreich, *Phys. Rev.*, **A41**, 4402 (1990).
[28] D. Schmidt, M. Schadt and W. Helfrich, *Z. Naturforsch*, **a27**, 277 (1972).
[29] K. T. Schell and R. S. Porter, *Mol. Cryst. Liquid Cryst.*, **174**, 141 (1989).
[30] S. Garg, S. Saeed and U. D. Kini, *Phys. Rev.*, **E51**, 5846 (1995).
[31] S. Garg, S. Saeed, S. Wild, E. Bramley and U. D. Kini, *Molec. Cryst. Liquid Cryst.* (in press).